Naval Research Laboratory

Washington, DC 20375-5000

(2)

NRL Memorandum Report 6506

Pacific Marine Radar Sea Scatter Experimental Results

DENNIS B. TRIZNA

Radar Scattering and Propagation Staff
Radar Division

August 22, 1989

SECURITY CLASSIFICATION OF THIS PAGE

REPORT DOCUMENTATION PAGE

Form Approved
OMB No 0704-0188

1a REPORT SECURITY CLASSIFICATION UNCLASSIFIED	1b RESTRICTIVE MARKINGS
2a SECURITY CLASSIFICATION AUTHORITY	3 DISTRIBUTION / AVAILABILITY OF REPORT Approved for public release; distribution unlimited.
2b DECLASSIFICATION / DOWNGRADING SCHEDULE	
4 PERFORMING ORGANIZATION REPORT NUMBER(S) NRL Memorandum Report 6506	5 MONITORING ORGANIZATION REPORT NUMBER(S)
6a NAME OF PERFORMING ORGANIZATION Naval Research Laboratory 6b OFFICE SYMBOL (If applicable) Code 5303	7a NAME OF MONITORING ORGANIZATION
6c ADDRESS (City, State, and ZIP Code) Washington, DC 20375-5000	7b ADDRESS (City, State, and ZIP Code)
8a NAME OF FUNDING / SPONSORING ORGANIZATION 8b OFFICE SYMBOL (If applicable)	9 PROCUREMENT INSTRUMENT IDENTIFICATION NUMBER
8c ADDRESS (City, State, and ZIP Code)	10 SOURCE OF FUNDING NUMBERS PROGRAM ELEMENT NO / PROJECT NO / TASK NO / WORK UNIT ACCESSION NO

11 TITLE (Include Security Classification)
Pacific Marine Radar Sea Scatter Experimental Results

12 PERSONAL AUTHOR(S)
Trizna, D.B.

13a TYPE OF REPORT	13b TIME COVERED FROM ____ TO ____	14 DATE OF REPORT (Year, Month, Day)	15 PAGE COUNT
		1989 August 22	30

16 SUPPLEMENTARY NOTATION

17 COSATI CODES			18 SUBJECT TERMS (Continue on reverse if necessary and identify by block number)
FIELD	GROUP	SUB-GROUP	

19 ABSTRACT (Continue on reverse if necessary and identify by block number)

Results are presented for a low grazing angle marine radar sea scatter experiment conducted in the Pacific Ocean. A wide range of wind speeds and directions resulted in non-equilibrium sea conditions, in contrast to a previous Atlantic experiment in which ocean waves were fully developed. Statistical properties of the radar echoes are parameterized by a dual-Weibull model versus wind speed and differ from the North Atlantic data. Results include:

(i) median sea spike cross sections were 15 dBm^2 at 2-deg grazing angle at X-band, 6 dB weaker compared to the Atlantic data; S-band sea spikes were 10 dB below the X-band results; grazing angle dependence above 2.5 deg was similar for all three data sets;

(Continues)

20 DISTRIBUTION / AVAILABILITY OF ABSTRACT	21 ABSTRACT SECURITY CLASSIFICATION	
X UNCLASSIFIED/UNLIMITED ☐ SAME AS RPT ☐ DTIC USERS	UNCLASSIFIED	
22a NAME OF RESPONSIBLE INDIVIDUAL Dennis B. Trizna	22b TELEPHONE (Include Area Code) (202) 767-2003	22c OFFICE SYMBOL Code 5303

DD Form 1473, JUN 86 *Previous editions are obsolete* SECURITY CLASSIFICATION OF THIS PAGE

S/N 0102-LF-014-6603

19. ABSTRACT (Continued)

(ii) the X-band distributed scatter amplitude and grazing angle dependencies were similar to the Atlantic experiment, but 2.5 dB stronger for 10-m/s wind speed; the S-band data varied similarly, but were 5.5 dB weaker than the X-band;

(iii) use of a time lag of 9 hours was required for best correlation of radar data with wind speed, suggesting roughness generated by long gravity waves caused the sea echo azimuthal variation for low grazing angles rather than local wind driven roughness.

A modified version of Wetzel's cylindrical plume scattering model satisfactorily describes the sea spike cross section characteristics. For the Weibull distribution representing distributed scatter, a composite scattering model produces neither the correct absolute cross section nor the correct X/S band ratio using Bragg scatter spectral densities derived from high grazing angle radar experiments. Thus, the surface turbulence from a broken crest on the front face of waves may be responsible for the scatter from area-distributed roughness.

CONTENTS

PACIFIC MARINE RADAR SEA SCATTER EXPERIMENTAL RESULTS

INTRODUCTION

In a previous report (Trizna, 1988), an X-band radar sea scatter experiment was described which was conducted in the North Atlantic Ocean over a one week period. During the one week period of the experiment the westerly wind direction was virtually unchanged and the wind speed changed relatively slowly. These data were considered to be collected under equilibrium conditions, i.e., the seas were considered as fully developed for the highest wind speeds reported with a minimum fetch of roughly two hundred miles for the corresponding wind direction. High air-sea temperature differences were found to occur, indicating highly unstable atmospheric conditions. For such conditions, sharp crested and breaking waves are expected to occur, both of which have been suggested as being responsible for radar sea spikes (Wetzel, 1987). In the North Atlantic, mean sea spike amplitudes were found to be as high as 18-dBm^2 at 2-deg depression angles, and 1-% occurrences as high as 30-dbm^2, for a cell size 10-m on a side. Results of the Atlantic experiment will be compared with data reported upon here.

This paper presents a similar analysis of a much larger data base for both X-band and S-band radar data, collected under more variable winds than in the Atlantic. For this reason, this data is probably more representative of the typical open ocean marine environment. The data were collected aboard the NOAA research vessel, Discoverer, operating in the Pacific Ocean. The wind and sea conditions were different for this experiment than for the North Atlantic case. Although wind speeds were reported as high as 30 m/s, winds were found to change either in direction or speed before the waves were fully developed. Atmospheric stability was found to be neutral, to mildly unstable, and wave breaking is not expected to be severe for such conditions. The data are analyzed in parallel with the North Atlantic experiment, and the results are compared for the two cases. Further results will be published separately, because of the large number of parameters considered here. Other results will include up-wind/downwind and crosswind/downwind NRCS ratios, and mean RCS variation versus wind friction velocity models.

ENVIRONMENTAL CONDITIONS

Figs. 1a and b show a plot of fetch and time requirements for fully developed seas replotted from a report by Neumann (1955). In Fig. 1a, the fetch required for a given wind speed to create fully developed waves can be estimated by the location at which a given curve reaches its flattened region. For this region, the longest wave period and length is generated and longer waves cannot be created. For example, for 30 knot winds, the maximum period is roughly 20 sec, with a 300 nm fetch required (as seen by the intersection of the 300 nm line with the 30-knot curve near the flattened region of that curve). In Fig. 1b one can see that no winds above 20 knots reach a final wave frequency in any time less than 60 hours. Hence, for times less than 60 hours, waves driven by winds greater than 20 knots are not fully developed. Minimum

Manuscript approved June 16, 1989.

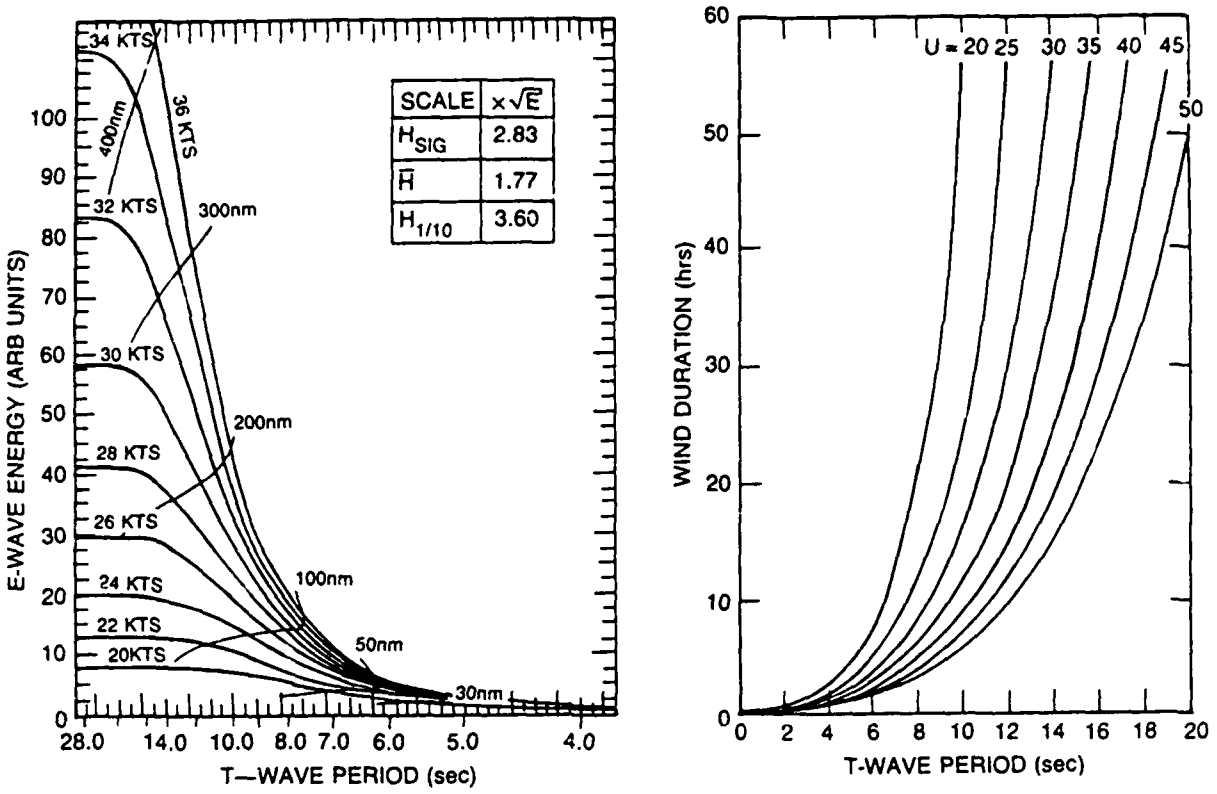

FIGURE 1. Plots from Neumann show the fetch/time relationship as seas become fully developed.

fetches for fully developed seas driven by 20 knot winds were reported by this Neumann work to be of the order of 150 nm, and longer for higher wind speeds.

Fig. 2 shows a plot of the wind speed, direction, and air-sea surface temperature difference for the periods during which radar data were analyzed. For the period between Julian day 53 through 58, for winds between 5 and 10 knots, the seas can be considered as fully developed. For the periods of winds 20 knots or higher, the winds do not blow for the minimum 60 hours required, and these waves were not fully developed. This is indicated now in anticipation of differences in sea spike characteristics found for the North Atlantic data and here.

RADAR DATA ANALYSIS TECHNIQUE

As for the North Atlantic experiment, the radar was calibrated by injecting pulsed r.f. energy from a microwave signal generator into the radar transceiver through a 20-db coupler. The receiver gain characteristics were determined by varying the input power over the 60-db dynamic range of the receiver. A calibration sphere was raised by helium balloon for absolute calibration of the entire transmit, receive, and digital recording chain.

Data were collected with an Analogic Data-5000 100-MHz sampling system with 64-KB on board memory, and stored on a Bering disk drive under control of an HP-86 computer through

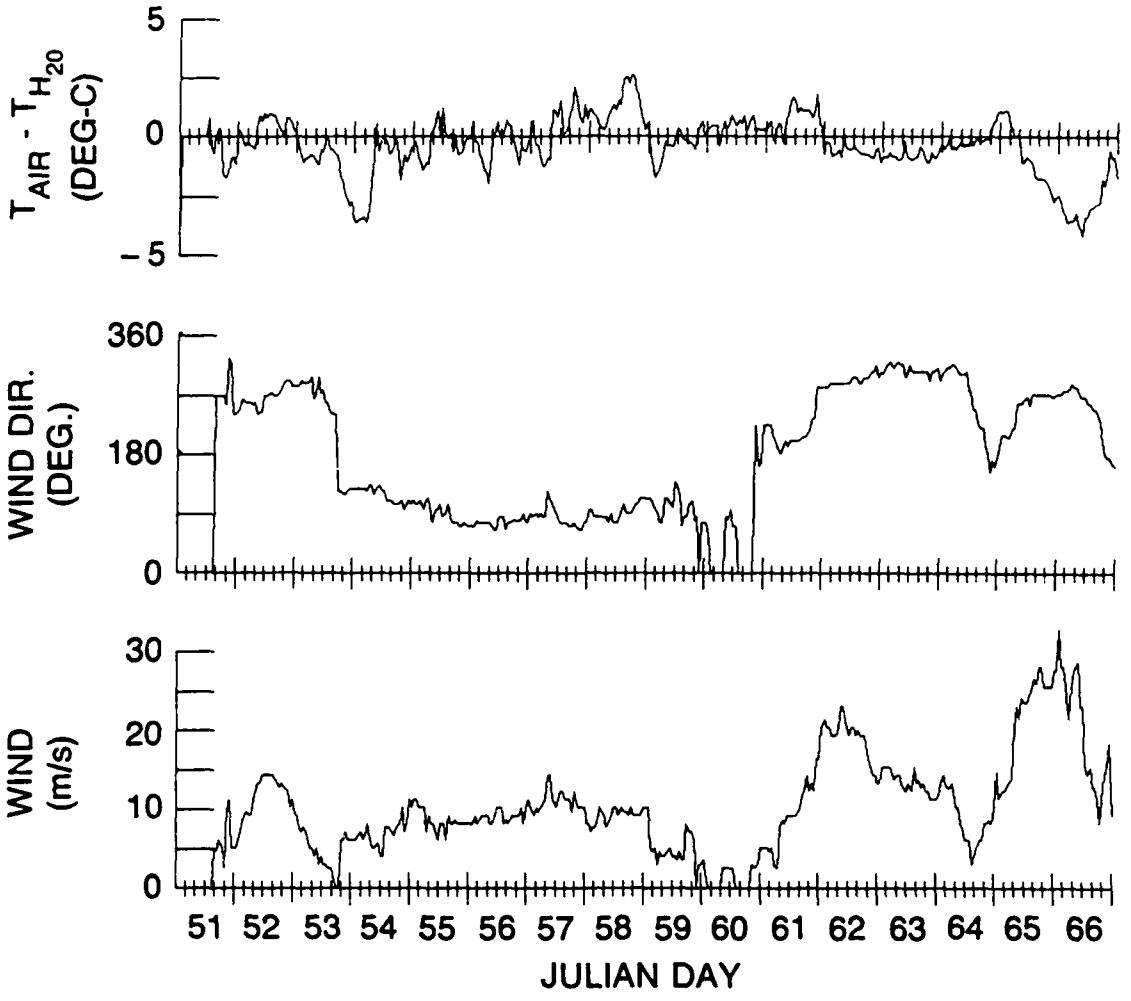

FIGURE 2. Plot of environmental data for the Pacific Experiment.

the HP-IB IEEE-488 bus. Data were backed up onto tape after the disk drive was filled. This combination allowed for better data quality than the tape system used in the Atlantic experiment, which could contaminate a full data run if a single tape error occurred within a file. In addition, the larger amount of on-board memory (vs the 4 KB of the Tektronix 7612D) gave more flexibility in collection speed. Overall, a higher fraction of data were uncontaminated than for the Atlantic experiment.

The analysis of the data began with determination of the peak of the mean echo power in azimuth. Because sea spikes were of interest, and are expected to dominate the mean at small depression angles, the lowest grazing angle was used to determine the peak angle for a given hourly collection. After the peak azimuth sector was found, the data chosen for determining the cumulative distribution of radar echo samples were those within a 60-deg sector centered on the peak azimuth. Ten range bins were analyzed, covering grazing angles from 1.4 to 6.3 deg. The normalized radar cross section (NRCS) was calculated for each selected sample and cumulative histograms of these values were stored and plotted on Rayleigh probability paper for each depression angle. On Rayleigh paper, Weibull distributions plot as straight lines similar to a Rayleigh, the latter being a special case of the former. Straight lines were fitted to

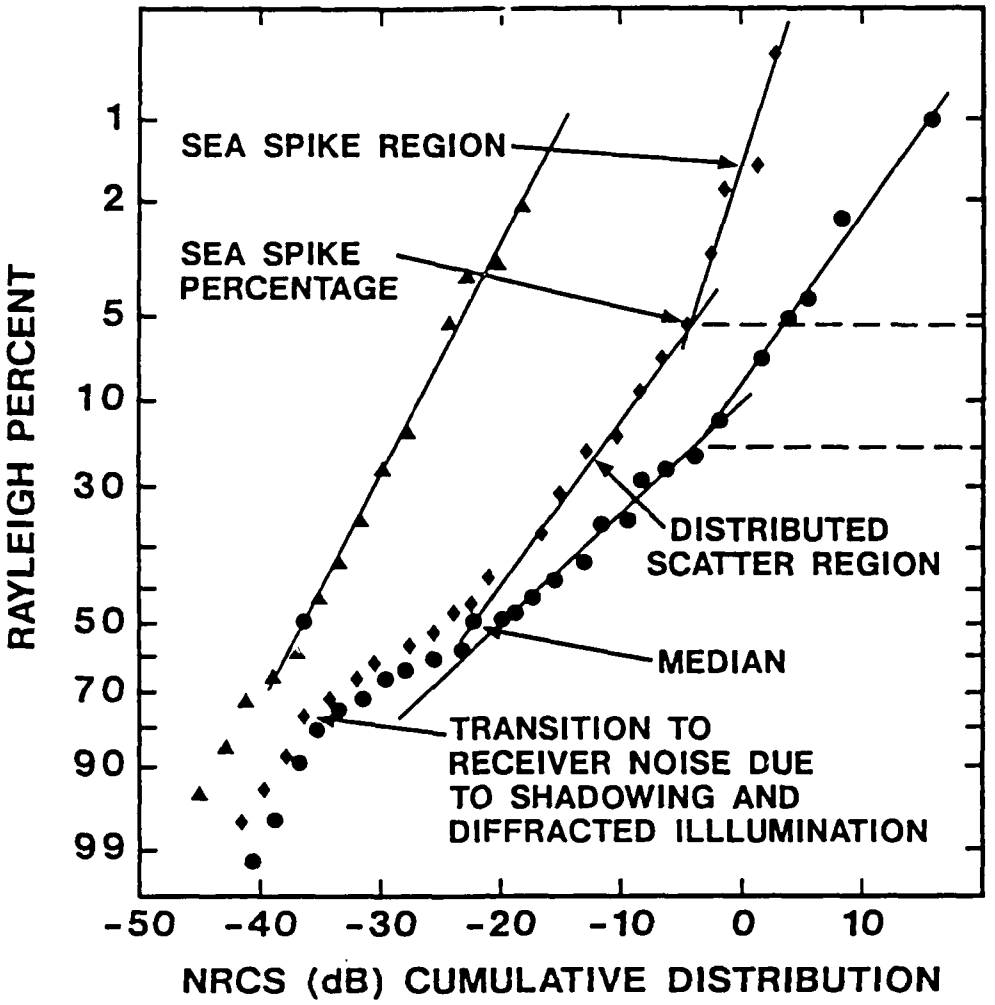

FIGURE 3. Cumulative histograms are plotted for X-band data for increasing wind speed, showing the changes in Weibull model fits.

two regions of the cumulative histogram data, each represented by independent Weibull distributions. Fig. 3 shows examples of three X-band cumulative distributions, indicating the behavior of the two Weibull regions with increasing wind speed.

In the Atlantic experiment, based on their different grazing angle behavior, each of these two Weibull distributions was identified with a different scattering mechanism: a distributed scatter source for the lower RCS Weibull distribution, and a localized scatter source for the higher RCS distribution. The higher amplitude distribution was associated with sea spikes, modeled in the earlier report by a spilling plume on the front face of the upwind side of a breaking wave crest. For each Weibull (linear) fit to the cumulative distribution on Rayleigh probability paper, two parameters characterize each of the two distributions: an amplitude and a slope. Furthermore, the transition from one Weibull contribution to the next occurs at the point of intersection of the two lines, with the percentage-coordinate of that point determining the percentage occurrence of sea spikes. For the fully-developed wave conditions which prevailed for the Atlantic experiment, this percentage of sea spikes was found to scale with wind speed in a manner similar to that of percentage occurrence of whitecap coverage, which has been studied by air-sea interaction experiments previously (See, for example, Wu (1979)).

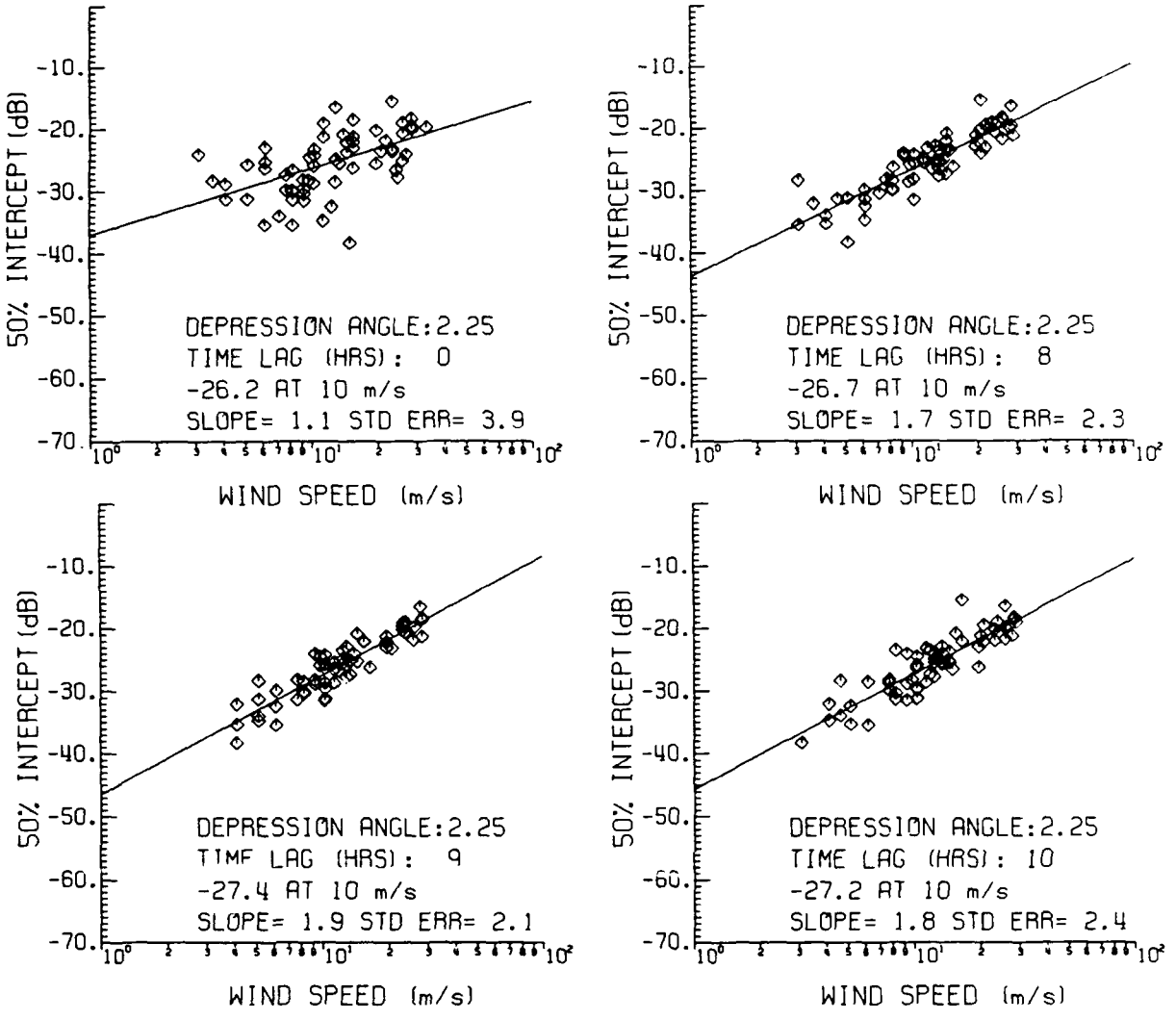

FIGURE 4. Median distributed scatter values vs wind speed for time lags of 0, 8, 9, and 10 hrs, showing time late effects.

RESULTS

Time Late Effects

The medians from the linear fit to the distributions are plotted versus wind speed in Fig. 4 for one of the grazing angles used. Fig. 4a shows cross section plotted versus wind speeds measured at identical times, i.e., with zero time lag. The scatter in the data is far greater than that found in the Atlantic results, but these data include much more variable winds and waves than found in the Atlantic data. In attempting to identify the source of this broad scatter in the data, a smaller subset was considered in detail, taken while wind speed increased and wind direction slowly shifted. Individual pairs of NRCS and wind speed values were tracked sequentially. The pattern of change of median RCS was noted to lag the wind change, and the analysis software was modified to introduce a time lag into the analysis. The data of Fig. 4a are

shown plotted in Figs. 4b, 4c, and 4d for time lags of 8, 9, and 10 hours, respectively, showing a marked improvement in correlation and the minimum standard error in the least squares fitting. The 9-hour lag was chosen as the lag for "best fit" correlation for the remainder of the analysis after giving similar consideration to the other grazing angles.

This time lag behavior can be explained qualitatively by the propagation of waves generated elsewhere traveling into the observation area. A quantitative analysis would require a study of movement of the large scale wind field, the propagation of the field, and the time of propagation of the ocean waves generated by these winds outside of the measurement area. This hypothesis suggests that low-grazing angle radar scatter is dominated by the large scale waves rather than local winds. Thus, the wind speed correlation with the mean RCS is just an implicit one, via the long ocean wave system which is generated. This is in contrast to the assumptions made in scatterometry, in which radar derived surface roughness is assumed to be entirely due to local winds.

Distributed Scatter - Corrections for STC

A difference in operational use of the radars aboard the Discoverer was required relative to that of the Researcher in the North Atlantic, which had two X-band radars. For the Atlantic experiment, one radar was used for marine navigation, while the second was dedicated to the sea scatter experiment with the display intensity turned off. A sensitivity-time-control (STC) circuit is normally utilized to avoid display saturation at the shorter ranges, by attenuating the received power levels at the short echo times. This, of course, affects the digitized signals of interest. The STC was minimized for the dedicated radar in the Atlantic experiment, because there was no possibility of burning out the display phosphor. Even with such minimization, two of the range bins were affected and required correction (Trizna, 1988).

Aboard the Discoverer, STC use was required for both radars which were used for normal operations. Hence, the STC was minimized but not eliminated, to prevent burning of the PPI screen phosphor for both radars at the shortest ranges. The ship's scientific staff were responsible for hourly collection of data on a not-to-interfere basis during the cruise. The X-band radar was considered the primary system for comparison purposes with previous results, and roughly twice as many hours of data were collected at X-band than at S-band. Both receivers were calibrated with a pulsed signal injected at a delay sufficiently beyond the STC-affected ranges, but the STC attenuation with range-delay was not measured in either case.

STC can be fully accounted for only when a dummy load can be inserted in place of the waveguide run to the antenna, because the time delays over which STC is applied are usually saturated by local echoes from other ships and buildings when the antenna is connected instead of a dummy load. Such echoes do not allow the full 60-db range of calibration signal at these short delays which are affected by STC with the antenna in line. With the antenna in the line, the calibration pulse is delayed to a range where no scatter is observed in the inter-pulse period, typically at longer ranges, which are not affected by the STC. This is the method used for both experiments as a dummy load could not be inserted into the line in place of the antenna. Thus

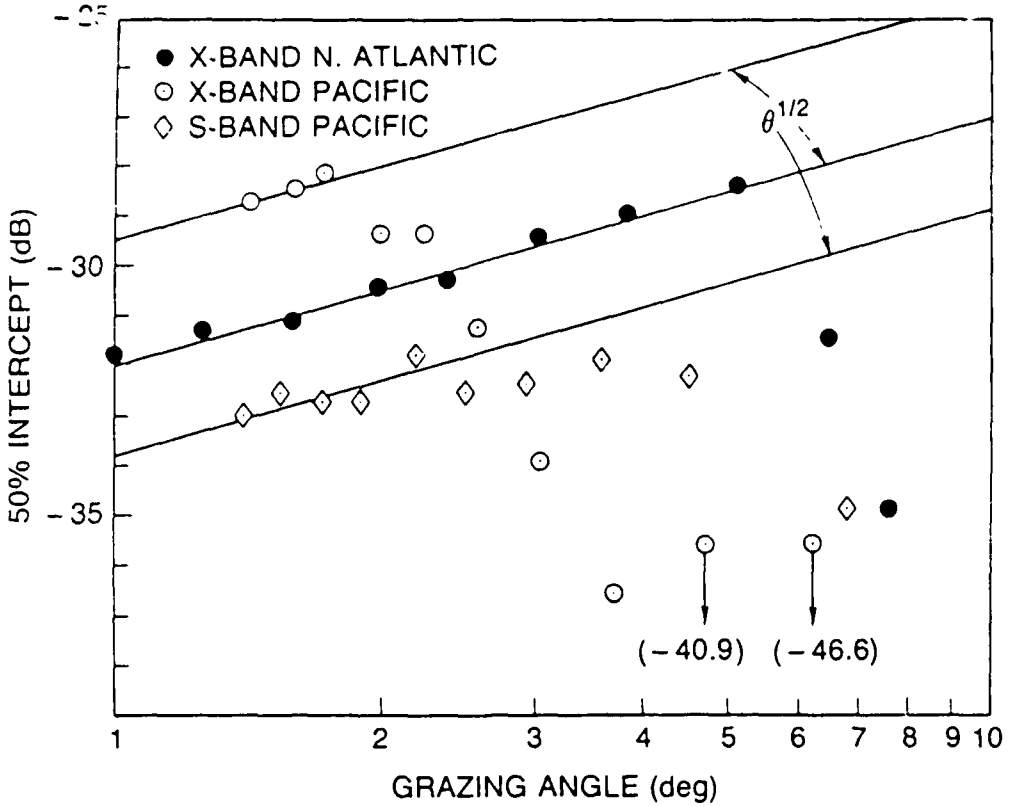

FIGURE 5. 10-m/s intercepts of plots of the type in Fig. 4, for 10 depression angles, for X- and S-band data and the N. Atlantic experiment. The data show similar magnitudes for the smallest depression angles, (longest range bins), but increasing STC attenuation effects for higher angles.

the effects of the STC were determined by consideration of the range dependence behavior of the sea echo data.

The existence of the small amount of STC attenuation required a correction strategy for the data at the shortest ranges. A technique is used similar to that employed for the Atlantic data. It is based upon the assumption of similar behavior for the two experiments of the "distributed scatter", (i.e., those radar echo samples caused by scatter sources evenly distributed across the radar cell, exhibiting constant normalized radar cross section with increasing radar cell area).

The plot of distributed scatter for the X- and S-band data is shown in Fig. 5. The X-band NRCS levels at the longest ranges and smallest grazing angles are expected to be unaffected by STC, for reasons discussed above. The first three X-band points exhibit a similar frequency dependence as that for the Atlantic data, shown with the solid line plotted through that data. However, the Pacific data lie roughly 2.5 dB above the Atlantic data at the lowest grazing angles, and this effect is assumed to be real. The fourth and successive points begin to fall off in magnitude due to STC, and it is assumed that these data vary with grazing angle similar to the North Atlantic data. For either experiment, according to a composite scattering model, the distributed scatter should vary with wind speed in a similar manner for all grazing angles. While the angular dependence may be a function of the particular small scale scattering model used, it is assumed that the same scattering model holds for both experiments. (See the further arguments made in the analysis of the Atlantic data - Trizna (1988)). Hence, the values for these last seven grazing angles affected by STC are adjusted to the line drawn through the first three data points, which is parallel to the line fit to the Atlantic data. This yields a correction in dB for each angle to be applied to the sea spikes and mean values to be considered later.

Similar STC effects occurred for the S-band data, also shown in Fig. 5. In this case the data are about three dB below the Atlantic X-data, again assumed real. Just the last five points require adjusting, again to the parallel line drawn through the unaffected points.

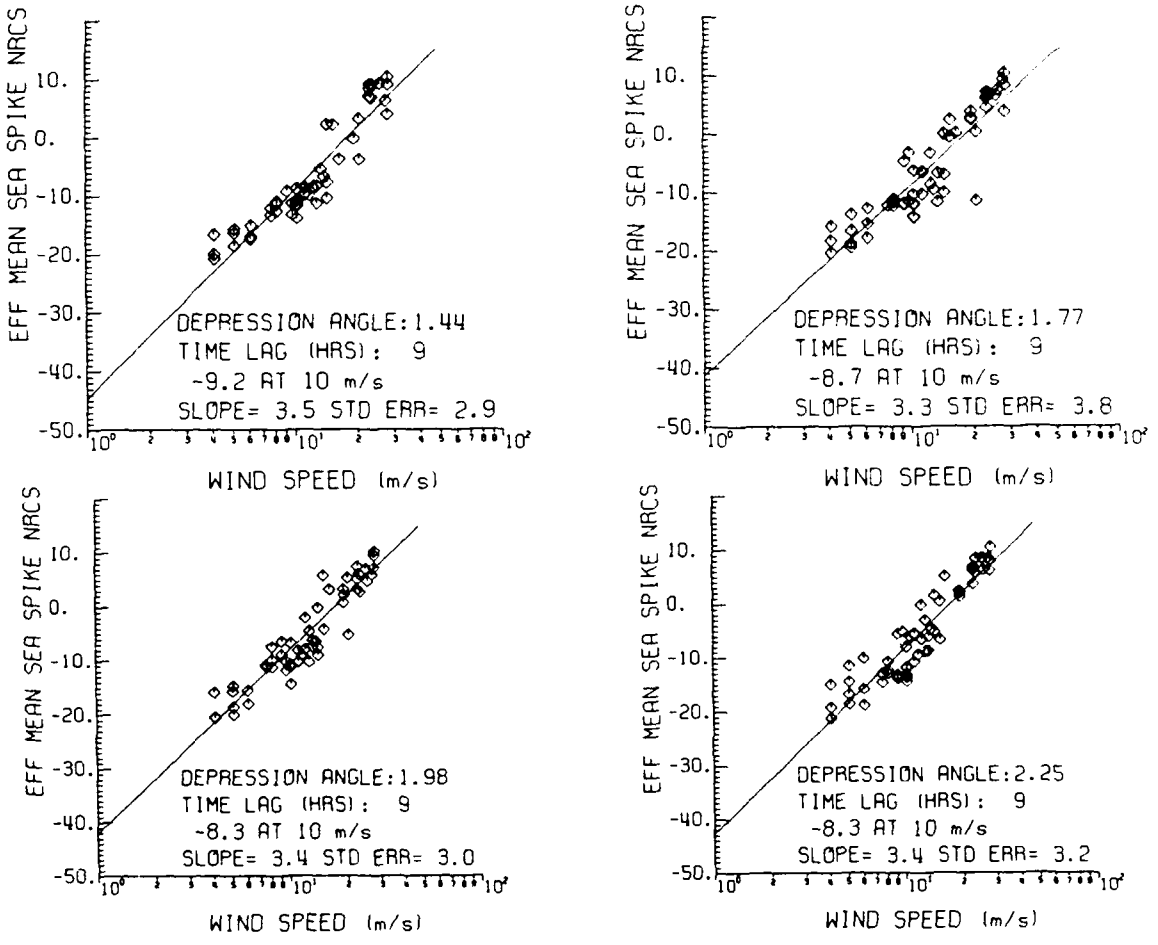

FIGURE 6a-c. Examples of sea spike effective mean values plotted versus wind speed, without STC corrections applied, for 4 depression angles.

Sea Spikes

i. Effective Mean Values

The effective mean sea spike value was defined in the Atlantic analysis as the dB-mean of the two-Weibull intercept and 1-% intercept of the linear fit to the sea spikes. While having questionable physical meaning, it is a convenient way of parameterizing the sea spikes for an empirical data base, and offers an estimate of the mean sea spike RCS. Figs. 6a-d show sea-spike effective mean NRCS values plotted versus wind speed for four of the ten depression angles used. These data also exhibit a much tighter distribution that the Atlantic data. No STC corrections are used for STC in this plot, but the 9-hr time lag is applied.

The 10-m/s intercepts of the linear fits to data such as these are plotted versus grazing angle in Fig. 7. The North Atlantic X-band data and Pacific S-band data are also included, and here the STC corrections have been applied. (Note that these data vary smoothly through the grazing angles with STC corrections, verifying validity of the correction technique.) For higher grazing angles, the Pacific data angle dependence is similar to that of the Atlantic data, but about 6 db weaker. A straight line with θ^{-2} slope has been drawn through each data set in this region. Note that the sharp rise in cross section which occurred near two degrees grazing angle is not evident in the Pacific data, while cross sections are very similar below 2 deg for the two X-band data sets.

The S-band data are seen to lie about 10 dB below the Pacific X-band data, and also fall off

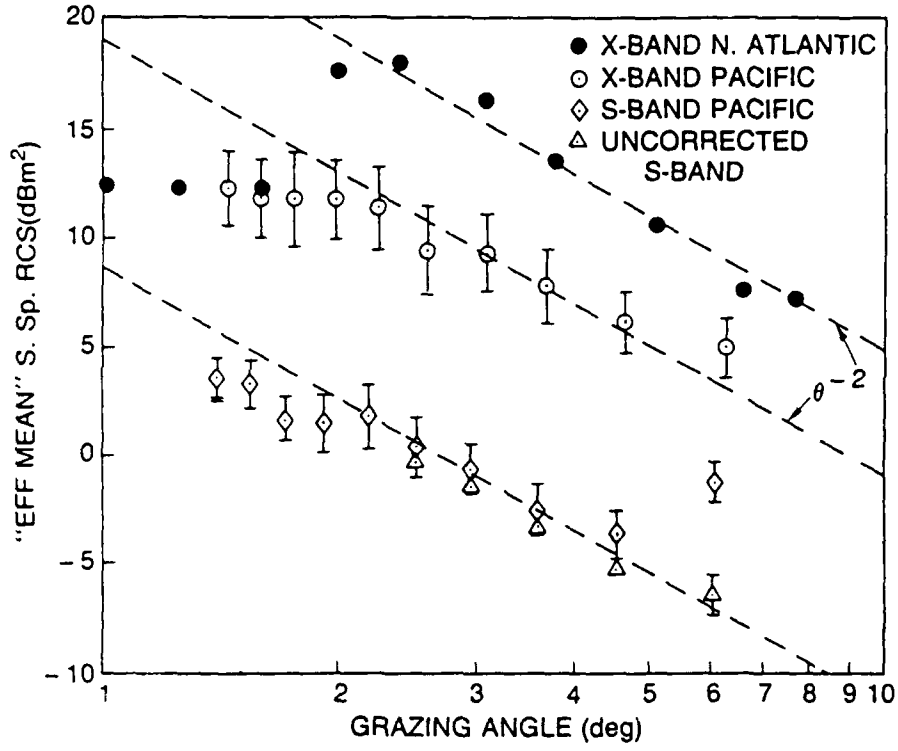

FIGURE 7. Plots of 10-m/s intercepts of sea spike effective means, (with STC applied) vs grazing angle for X- and S-band data, with N. Atlantic results.

with grazing angle with a θ^{-2} slope. Uncorrected S-band data are also shown, and fit the same grazing angle behavior for the most part. Note that the last S-band STC correction was 5 dB, while the same X-band correction was 21.1 dB. Thus, the STC circuit for the S-band radar does not attenuate as strongly as for X-band because of the generally weaker clutter return for the S-band frequency.

In the Atlantic analysis, the θ^{-2} slope beginning at 2.5 deg grazing angle was suggested to be due to a fixed cross section scatterer beginning to fill the radar beam in the cross-beam dimension at the corresponding range. The scatterer was modeled as a quarter-cylinder shaped feature or group of features on the front face of the wave, representing a spilling breaker. Thus the target changes from a discrete scatterer of fixed width, wholly within the radar beam, to a partially distributed scatterer filling the beam in the cross-range dimension. For the radar antenna height and the observed 2.5-deg grazing angle, the range where this behavior starts is 570 m. Using a 1-deg beamwidth, the width of the beam at this range is roughly 10 m. The cylindrical radius required to explain the Atlantic RCS magnitudes were of the order of 3 to 6 cm, assuming a perfectly shaped single cylinder over the 10-m width. For several narrower cylindrical features distributed across a 10-m width, larger radii are allowed. Similarly, any deformations from a perfect cylindrical shape would allow a larger radius. Further comparisons with scattering models will be made later.

ii. Sea Spike 1-% Intercepts

The 1-% intercepts for the X- and S-band data are shown in Fig. 8, and these are independent of any Weibull model fit. There is an even larger magnitude difference between these X-band Pacific and Atlantic data above 2 deg when compared to the sea spike effective means considered in Fig. 7. This is result of the broader width of the distribution of sea spikes for the Atlantic data above 2 deg (increase in Weibull-B), to be shown in the next section. Note that the X-band data at the lowest grazing angles have roughly a 5-dB difference from Pacific to

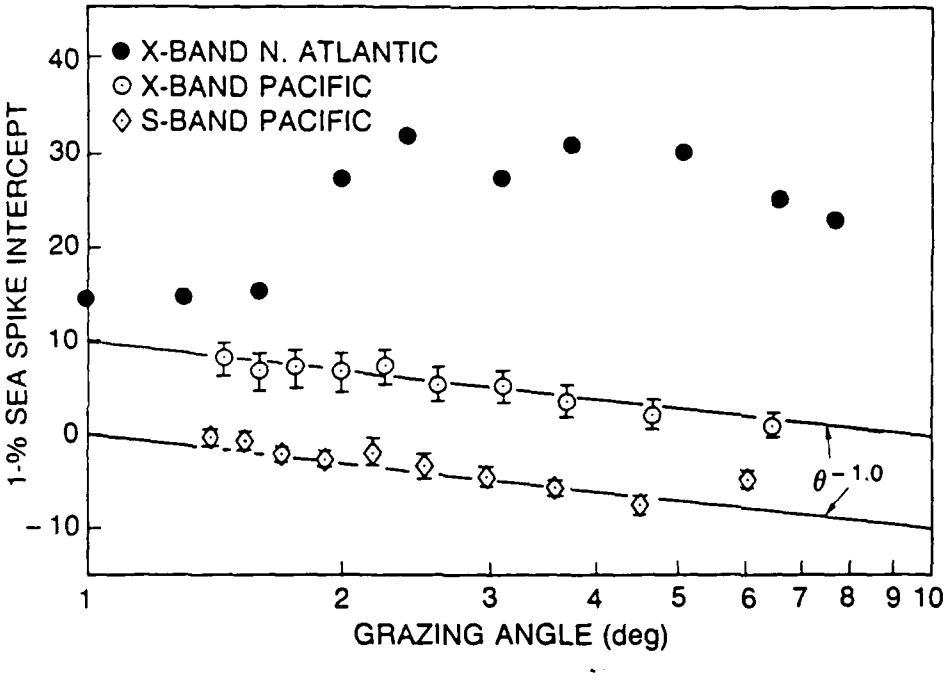

FIGURE 8. Plots of 10-m/s intercepts of sea spike 1-% values are shown plotted versus depression angle; Pacific X-band values show similar slopes and a 2-deg RCS increase as for the N. Atlantic results.

Atlantic, relative to the nearly equal values for the "effective mean" for the two cases and lowest angles. The rms error in the Pacific data is very narrow compared to the Atlantic, an indication perhaps of weaker wave breaking. An angular dependence of θ^{-1} has been fitted by eye to the data for each case. One can estimate that the two lines flatten for angles below 1.5 deg, in similar fashion to the Atlantic data.

Weibull Slope Parameters

For full characterization of the statistics of the scatter using the two-parameter Weibull distribution, a parameter which gives a measure of the width of the distribution is the B-parameter. The cumulative probability distribution function of linear normalized radar cross section (NRCS) values **x** is represented by the Weibull distribution in Eq. 1:

$$p\{x\} = \exp(-x^B/A) \qquad (1)$$

This parameter is convenient for applications to the detection of targets in clutter. The Weibull B-parameter is measured as the slope of the linear fit to the log of the NRCS cumulative distribution plotted on log-log Rayleigh probability paper. In some applications, the distribution studied is one of voltages, for which B = 2 yields a Rayleigh distribution. In our analyses, we have studied the radar cross section, determined from measurements of received power, for which B = 1 results in the Rayleigh distribution.

Weibull B-slopes at 10-m/s wind speeds are shown plotted in Figs. 9 and 10 for the distributed scatter and sea spike regions, respectively. For the Pacific data, both sets are relatively constant with depression angle, compared to the sudden increase in B at 2-deg grazing for the Atlantic data. As a larger B-parameter represents a wider range in the distribution function, this increase in B corroborates the observation in the previous section showing higher X-band 1-% intercept differences between Pacific and Atlantic data above two degrees, as the 1-% values occur out in the tail of the distribution. In the case of the Pacific data the Weibull parameters are remarkably constant with depression angle for both distributed scatter and sea spike distributions. All the B data appear to cluster between 1.75 and 2.25 for the distributed scatter, and between 0.75 and 1.0 for the sea spike B, suggesting a Rayleigh distribution here. Note that the rms spread in the Atlantic data was roughly the same as that of the X-band Pacific data. One might expect the width of both partial distributions to be larger for the Atlantic data if the waves were closer to fully developed than in the case of the Pacific experiment. Assuming a composite model as responsible for the distributed scatter, the larger crest to trough heights of the Atlantic wave conditions would be expected to introduce a wider range of local depression angle modulation of the NRCS, resulting in the wider distributions for the Atlantic distributed scatter. Likewise, one would expect more intense wave breaking for the Atlantic data, resulting in a wider distribution of NRCS values for this contribution to the distribution as well.

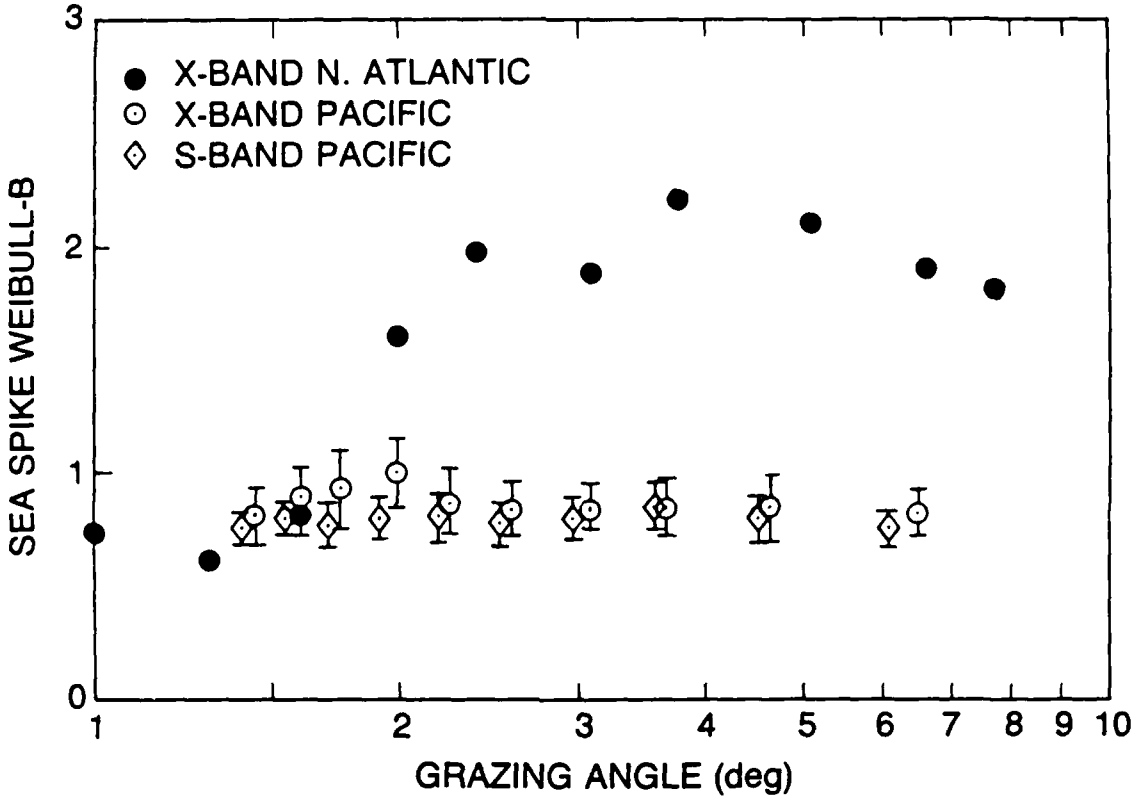

FIGURE 9. Plots of B-values of distributed scatter at 10-m/s wind speeds vs depression angle for X- and S-band data, as well as N. Atlantic results.

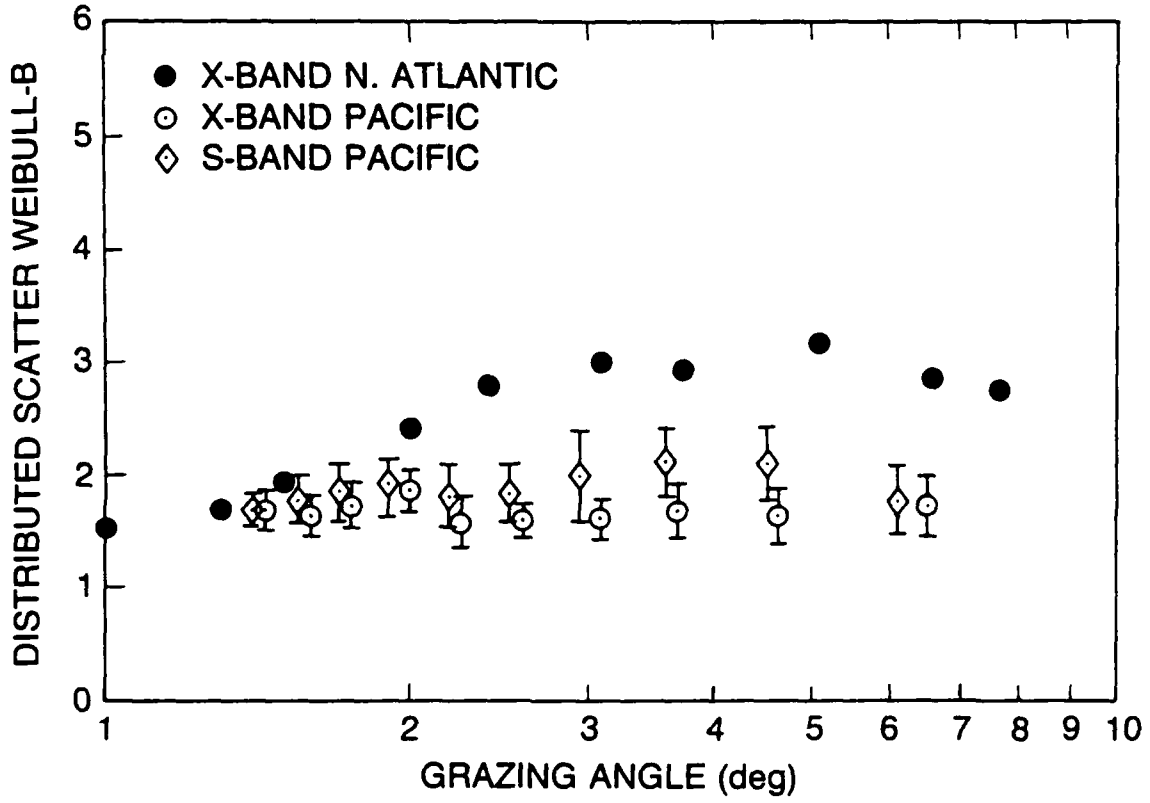

FIGURE 10. Plots of B-values of sea spike scatter at 10-m/s winds speeds vs depression angle are shown for X- and S-band data.

Wind Speed Dependencies of Medians, Means, and B-Parameters

The final parameter necessary to characterize the sea scatter by Weibull fits are the wind speed dependencies of the medians, means and the Weibull parameters. Because of the log-log method used to plot the data versus wind speed, the same as that used in scatterometry and other sea clutter models, the wind speed dependencies follow as exponential, of the general form:

$$F(W) = F(10\ \text{m/s}) + dF/dW * \log(W/10) \qquad (2)$$

where W is wind speed, F(W) is the log of the RCS for the case of effective mean sea spike RCS and 50%-intercepts or medians, and dF/dW is the measured slope, giving the exponential dependence. However, for the B-parameters, F(W) is just B.

The exponents, dNRCS/dW, are shown in Figs. 11 and 12 for the medians and sea spike effective means, respectively. For the median NRCS, both S and X-band exponents are nearly constant, approaching 2 for increasing grazing angles for the Pacific data, in contrast to the

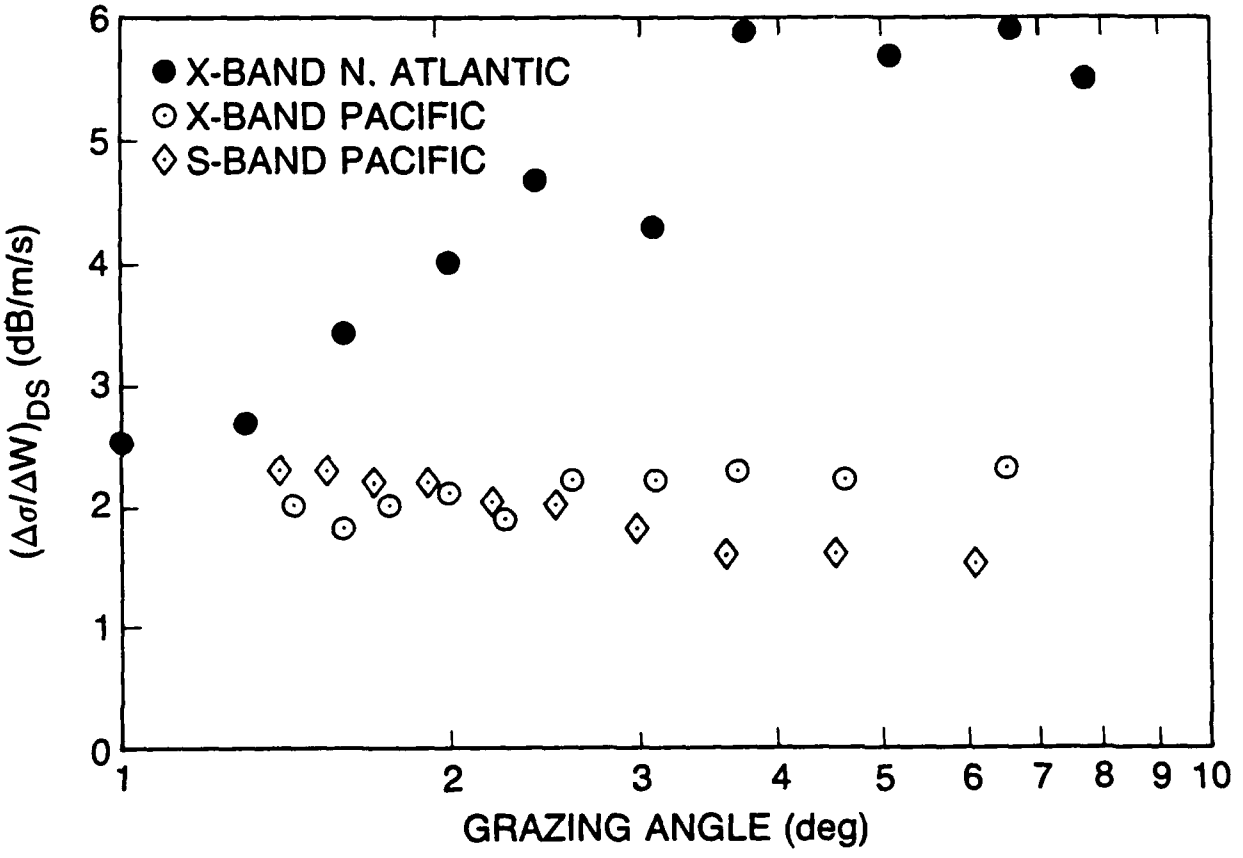

FIGURE 11. Wind speed exponents for distributed scatter medians vs depression angle for X- and S-band data.

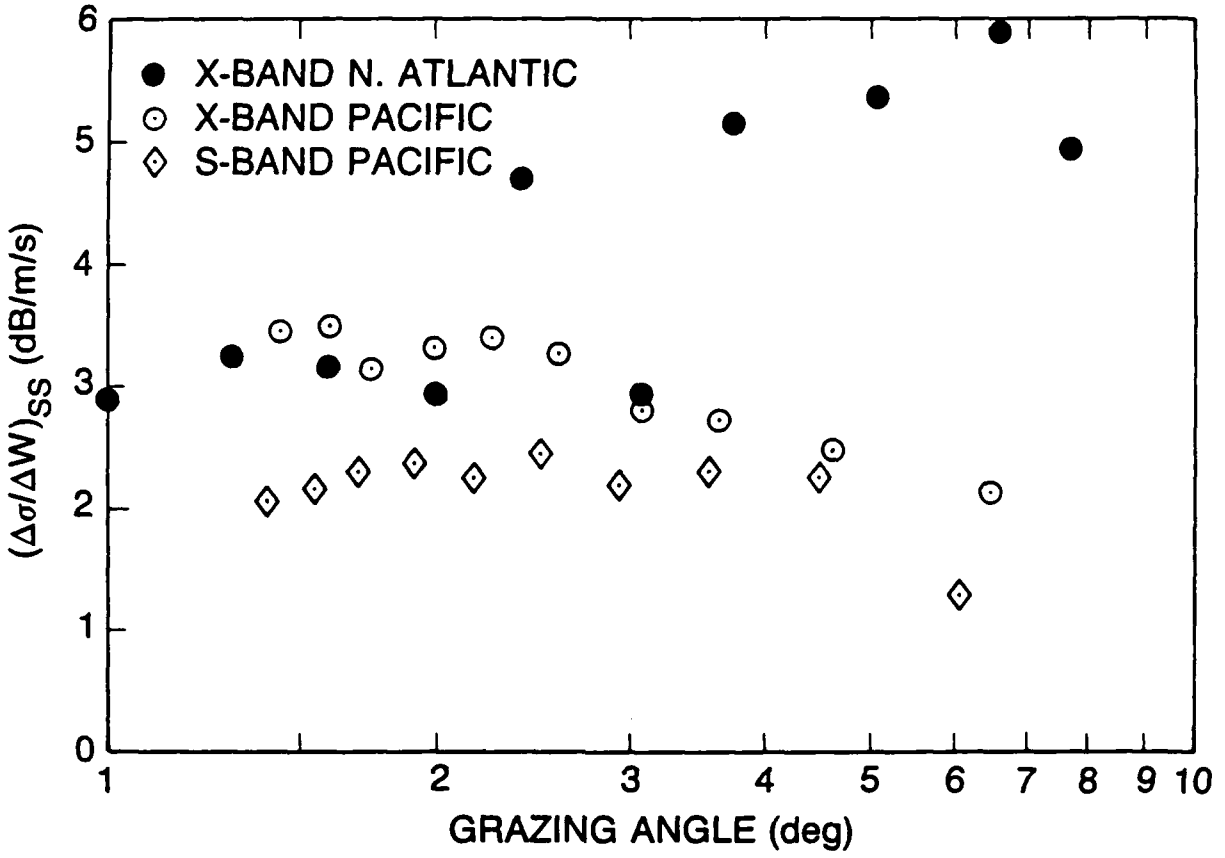

FIGURE 12. Wind speed exponents for sea spike scatter effective mean values vs depression angle for X- and S-band data.

higher values near 3 encountered in the Atlantic X-band data. For the S-band data, the exponent appears to be approaching 1 for the higher angles.

For the sea spikes, the wind speed exponents are much smaller than the Atlantic results for grazing angles above 2 deg. For angles less than 2 deg, the X-band data for the Atlantic and Pacific data appear very similar, as with other variables studied earlier, suggesting the same scattering model in this region for the two experiments. These results agree with those reported by de Loor and Hoogeboom (1982) for X-band long-term RCS means for 1 and 10-deg grazing angle. For S-band data, the exponents appear to cluster about 2 and are relatively constant with grazing angle, except for the drop off at the last angle again.

The wind speed exponents of the Weibull parameters are shown in Figs. 13 and 14 for distributed scatter and sea spikes respectively. These exponents are generally less than one, showing a very weak wind speed dependence, except for the very lowest grazing angles. Five

of the S-band data above 2 deg were slightly negative, but these data showed very large rms spreads and are assumed to be near zero and were not plotted.

It would appear that derivation of these statistical properties from first principles is not possible at this time, and that they can only be modeled by simulation of deterministic realizations of the surface with assumptions about non-linear scattering features responsible for sea spikes, their probability of occurrence, and their scattering cross sections.

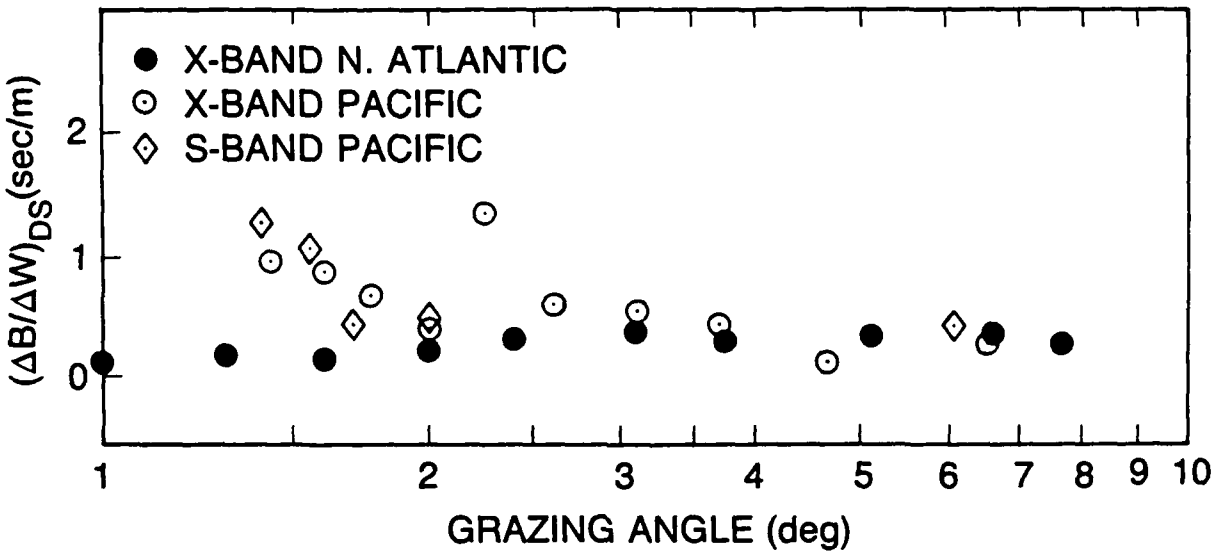

FIGURE 13. Wind speed exponents for distributed scatter Weibull B-values vs depression angle for X- and S-band data.

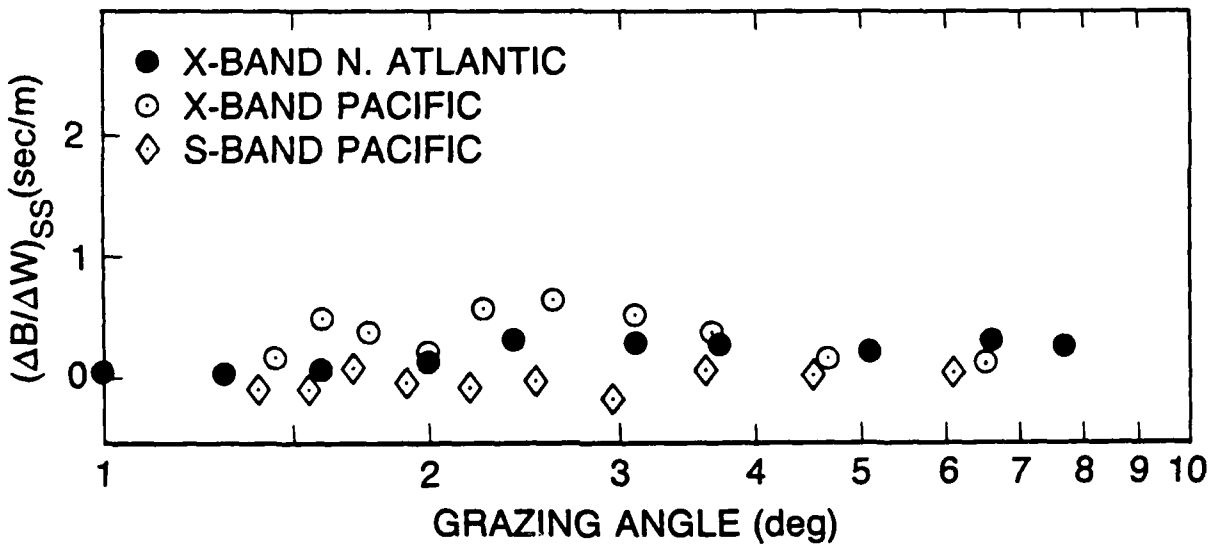

FIGURE 14. Wind speed exponents for sea spike Weibull B-values vs depression angle for X- and S-band data.

TESTING OF SCATTERING MODELS

One can utilize the X and S-band results for the two experiments for comparisons with radar scattering models. There are four aspects to consider: the X-band median differences between the Atlantic and Pacific data, the X/S-band cross section ratio for the Pacific median scatter, and the X/S-band ratio for the sea spikes, and the grazing angle dependencies of sea spikes.

Distributed Scatter

i. Ratio of Atlantic and Pacific X-Band Medians

Consider the median scatter shown in Fig. 5, which is used as the absolute amplitude calibration for the sea spike data. In particular, consider first the 2.5 dB difference in the X-band data from the Atlantic and Pacific experiments. We assume that this region of distributed scatter in the distribution function is due to wind driven roughness, with no assumptions as to the particular scattering mechanism. We only assume that it is due to distributed scatterers filling the illuminated area because of the very weak dependence on area in going from the shortest ranges to the longest.

Because these data were collected in the upwind direction, the illuminated surface roughness lies on the forward face of waves and in the lee of the wind. Figure 15 shows this geometry, with the wind blowing right to left. The wind acts primarily on the back face of the waves, as demonstrated by Sun and Wu (1984), and Okuda, et al, (1977). Hence, if the waves were steeper in the Atlantic, then one might also expect stronger sheltering of the wind on the leeward face, producing weaker distributed scatter there. Such a sheltering effect is assumed to be responsible for the lower local wind friction velocity on the leeward face reported by Sun and Wu. No open ocean measurements of wind friction velocity variation along the long-wave profile have been made analogous to the tank measurements of Sun and Wu, so that the 2.5 dB difference in our radar data cannot be verified. Nonetheless, this difference agrees with the expected behavior suggested by quantitative wave tank measurements, if one accepts the assumption of stronger wind sheltering due to steeper waves. Because of the lack of quantitative data on this sheltering effect, the observed 2.5 dB difference cannot be used as a test of Bragg scatter models. For this we must consider the X/S-band ratio.

FIGURE 15. The geometry for upwind radar illumination from a shipboard radar is shown, wind and waves moving right to left. Wave breaking occurs on the leeward face, and sheltering of this face by steep waves is expected as described in the text.

ii. X/S-band Ratio of Pacific Medians

The X/S-band ratio of median scatter for the Pacific data in the same figure is roughly 4.3 dB. If one utilizes the composite Bragg scatter model for this region, then the X and S-band NRCS values are proportional to the spectral amplitude of the Bragg-resonant directional wave spectral component of the roughness. As no open ocean wave-number spectra have been measured in the 1 to 10-cm wavelength gravity-capillary transition region, we must rely on wave models for estimates of these spectral amplitudes. Lee and Fung's model for the wave number spectrum in this transition region can be used (1984). It was developed using K-band radar NRCS measurements and uses the Bragg scatter model to estimate the spectral amplitudes at the single K-band resonant wavenumber. Using radar measurements for five wind speeds, they inferred the absolute values of the spectrum at a 2.16-cm radar wavelength for five different friction velocities. The transition to the gravity wave region of the spectrum was extended in a continuous fashion from K-band to the gravity wave region, covering the X and S bands of interest here.

Fig. 16-a shows the behavior of the wavenumber spectrum in the wave number region of interest using this model. The log of the ocean wave number region for K/X/S band frequencies are 0.765, 0.594, and 0.0992, respectively. It is seen from Lee and Fung's figure that all three radar-resonant wave numbers lie in a region where both the slopes and absolute levels of the curves are sensitive to the wind friction velocity. Quantitative comparisons can be made using Fig. 16-b, where these curves are expanded to show the variation more accurately. A 10-m/s wind speed at 10-m altimeter height appropriate to our radar data yields a wind friction velocity of 32 cm/s using Large and Pond's drag coefficient (See Trizna (1988), for a description of the friction velocity-wind velocity relationship). No angular spreading function is used as waves at these wavelengths are uniformly distributed in azimuth. Using the curves of Fig. 16-b, extrapolating linearly between the curves for 12 and 49 cm/s, and using 0.099 and 0.59 for the S and X-band log-K intercepts, the spectral amplitudes are estimated to be -20.2 and -31.7 dB-cm^2/(rad/cm).

The ratio of NRC values is given by

$$NRCS_X/NRCS_S = (K_X/K_S)^{-4}\, S(K_X)/S(K_S) \qquad (3)$$

In decibels the two terms on the right hand side are 19.8 and -11.5, resulting in a theoretically expected cross section ratio of 8.3 dB for our results. This is 4 dB greater than our measured value of 4.3. Such a difference is probably within the experimental error of the two experiments, ours and that used to derived the results by Lee and Fung. (Note that using a composite model with a mean local incidence angle of 70 or 80 deg relative to the normal, due to the tilt by the long waves, would shift the resonant wavenumbers in a linear fashion, but not out of the region of Fig. 16-b, so that the calculated ratios are not altered significantly by this consideration.) One possible explanation for the 4 dB difference is that our data represent a selective sampling of the roughness on the front face of the wave, while the Lee and Fung model is derived from scatterometer data which averages over many long waves. Trizna & Wu (1989) have suggested forward face roughness due to wave breaking as one of two sources of long-wave phase variable roughness in a new model for the modulation transfer function. Such a source would be selectively chosen as the source of distributed roughness observed here as

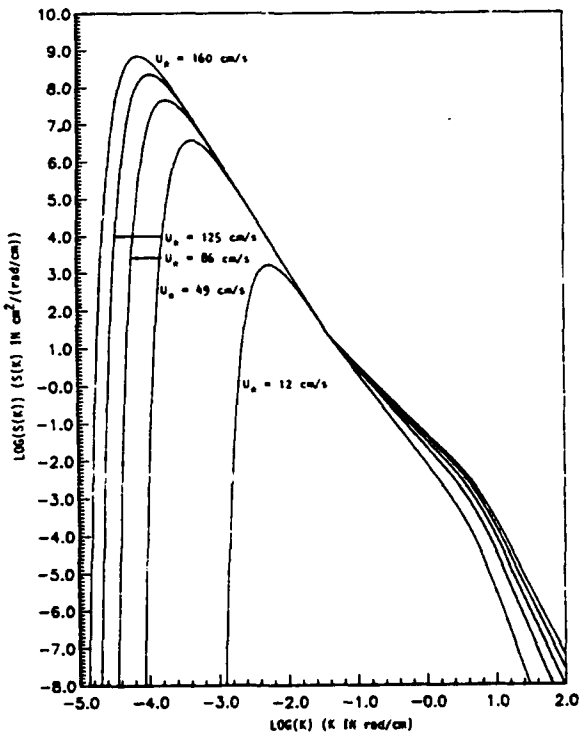

*FIGURE 16a. The wind speed dependence in the gravity-capillary region of the wave spectrum proposed by Fung and Lee.**

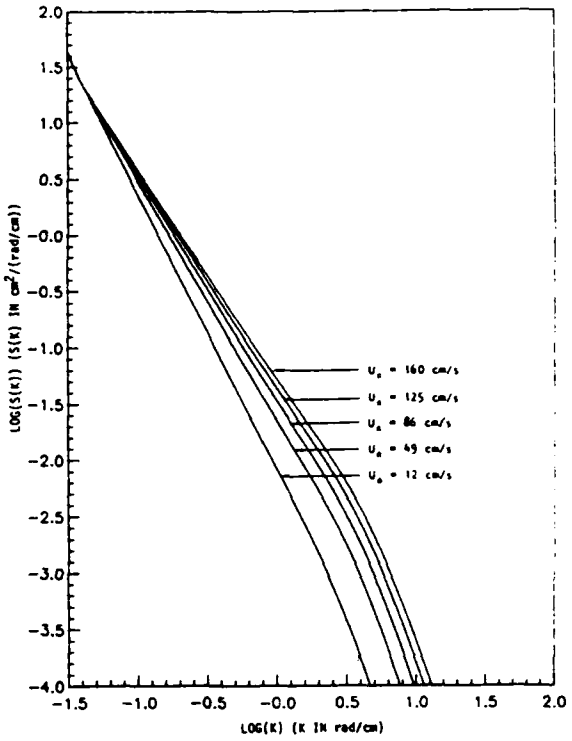

FIGURE 16b. The region in the previous figure is expanded to show the detailed dependence in the wavenumber range of interest. †

well. Such roughness would probably be the result of turbulence rather than linear waves on the surface assumed by composite radar scattering models, and is only one of two or more sources of roughness measured in the Lee and Fung model. Thus, interpretation of our distributed scatter results using this spectral wave model is in general agreement with a composite Bragg scatter model considering all of the above caveats and uncertainties.

Note that while Bragg scatter is used in the formal development of the composite model, the Lee and Fung wave model's use of K-band radar data is empirical, and thus is independent of a radar scatter model. Wetzel (1988) has suggested a surface populated by small wave crests, modeled by wedges, which do not satisfy the assumptions of small wave height-to-wavelength required for applying Bragg scatter. Such a model fits the data generally used to compare with the composite model as a function of grazing angle just as well.

*Fig. 1, page 167 from "A Semi-Empirical Sea-Spectrum Model for Scattering Coefficient Estimation," by Adrian K. Fung and Khim K. Lee, from IEEE Journal Of Oceanic Engineering, Vol. OE-7, No. 4, October 1982, published by the IEEE Council on Oceanic Engineering, Copyright 1982. Used by permission.

†Fig. 2, page 167 from "A Semi-Empirical Sea-Spectrum Model for Scattering Coefficient Estimation," by Adrian K. Fung and Khim K. Lee, from IEEE Journal Of Oceanic Engineering, Vol. OE-7, No. 4, October 1982, published by the IEEE Council on Oceanic Engineering, Copyright 1982. Used by permission.

Sea Spike Model

Consider now the sea-spike behavior for the three sets of data of Figs. 7 and 8. There are two features of these curves which can be used in testing scattering models: the similar grazing angle dependencies for all three data sets beginning at the same 2.5 grazing angle for the X-band data, and the 10-dB difference between the X and S-band data. Assuming that sea spikes are associated with wave crests, it follows that the sea spike differences between the Atlantic and Pacific data are due to variation in the character of the crests of the long waves created under the two different sets of wind conditions. With the much longer fetch and time of constant wind direction for the Atlantic data, one might expect longer crested waves and much more vigorous wave breaking in that case.

i. Grazing Angle Dependence

The model proposed to explain the Atlantic sea spike grazing angle dependence invoked a mean 10-m wide cylindrical crest, causing the -2 power grazing angle variation beginning at a 570 m range/2.5-deg grazing angle. If one adopts the same model for the Pacific data, then the same 2.5-deg onset of the -2 falloff for both X-band data sets requires 10-m wide crests means. Using this model, differences in absolute amplitudes between the Atlantic and Pacific data must then depend upon specific differences in the range-dimension variations of the crests encountered for the two cases. These include the cylinder radii and surface coherence or a random roughness function, representative of a mottled structure on the scattering surface which reduces the specular scatter from the cylinder. Using the expression for the RCS for a cylinder, $RCS = kaL^2$, where 'a' is the cylinder radius and L its length, postulating a 10-m wide crest requires a radius of a centimeter or less to fit the observed RCS values of Fig. 7. However, this wavelength no longer satisfies physical optics, which the above RCS expression was based upon. Random variation along the cylinder, or several independent spilling features randomly phased down the face of the wave as proposed by Wetzel (1986) could lessen the surface coherence as seen by the radar. Such randomness could cause a reduction in the cross section for both Atlantic and Pacific data. A randomness factor of the order of 6 dB would thus allow radii of curvature for the cylinder of the order of 6 cm for the Pacific data, and 24 cm for the Atlantic data. Such dimensions are not unrealistic for spilling crest features.

ii. X/S-band Ratios for Sea Spikes

Consider next the X/S-band ratio for the sea spike RCS. In both Figs. 7 and 8, this ratio is roughly 10 dB. To strengthen this argument, the grazing angle dependencies of sea spike means and total means are plotted versus grazing angle in Fig. 17 for X and S-band data. (The sea spike mean for each cumulative distribution was calculated by simply summing the linear RCS values which occur above the RCS intercept of the two Weibull fits, and dividing by the number of sea spikes in the histogram. These results will be described further elsewhere.) The ratio of the θ^{-1} dependence fits to each data set is also roughly 10 dB.

This is very close to the ratio of $(K_x/K_s)^2$, which implies a K^2 dependence for the sea spike scatterers. Scatterers which produce a square-law wavenumber dependence are flat plates at normal incidence and corner reflector dihedrals. A $(K_x/K_s)^1$ dependence is given by the

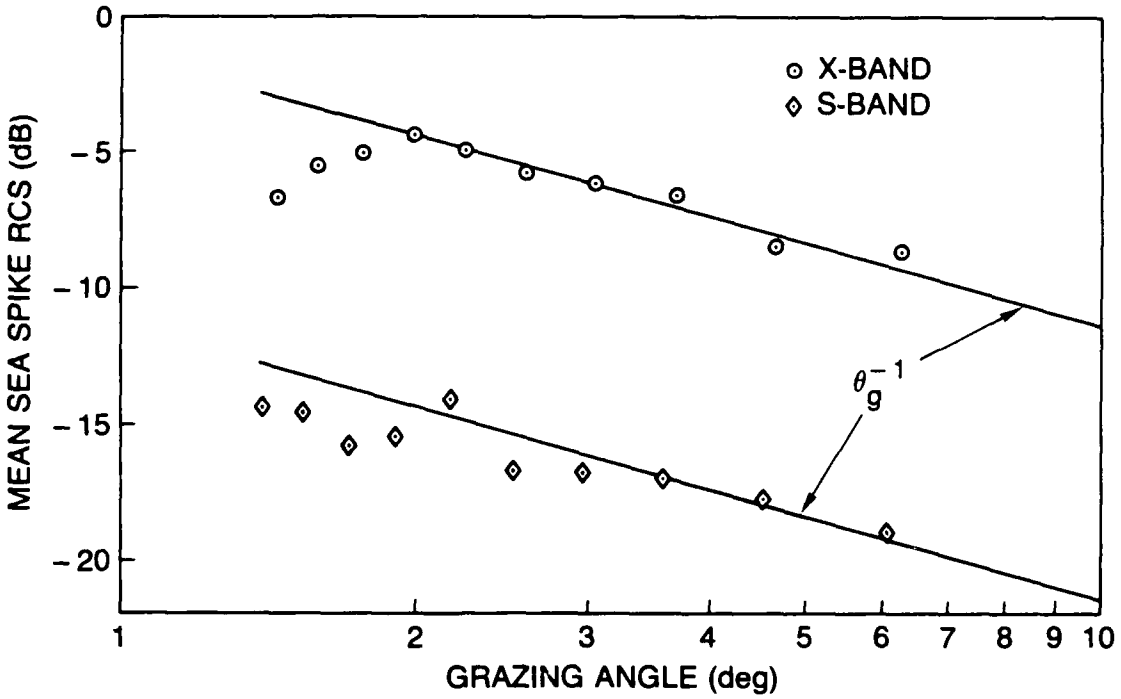

FIGURE 17. Sea spike true mean 10-m/s intercepts are plotted vs depression angle for X- and S-band data, and show a variation similar to that for the median values shown earlier, particularly the 2-deg sudden increase.

cylinder, where the region of specular scatter is reduced to a line of normal incidence from the full surface area of the plane. For the sphere, where the region of normal incidence is reduced to a point, there is no wavenumber dependence. In all of these cases, physical optics is assumed. This square-law wavenumber dependence is in partial agreement with Wetzel's plume model, which was considered in the Atlantic analysis, and is shown again here in Fig. 18a. However, there it was rejected in favor of a cylinder with toe line intersecting the surface with either a 0-deg (Fig. 18b) or a 2-deg (Fig. 18c) angle between the surface normal and the horizontal. The latter was invoked to explain the sudden increase in RCS which occurred at 2 deg grazing angle. It would intuitively appear that the 90-deg angle of the plume face to the tilted long wave surface in Fig. 18a would not be stable hydrodynamically.

All of these scattering models are very idealistic, and nature probably does not present such sharp intersections of water surfaces. Forcing additional models can only be considered as more speculation at this point. What is now necessary is more experimental work in defining the surface contour of representative surface features accurately with in-situ instrumentation, along with simultaneous multi-parameter radar measurements, such as polarization and/or radar frequency diversity, which provided a very useful source of comparison in this data. Secondly, the theoretical problem of radar scattering from a family of such surfaces should be solved exactly, without forcing the physical optics approximation, as the radii of curvature for cylindrical models considered here are of the order of a radar wavelength. It appears that understanding the experimental data requires more than first order scattering approximations as solutions to the problem.

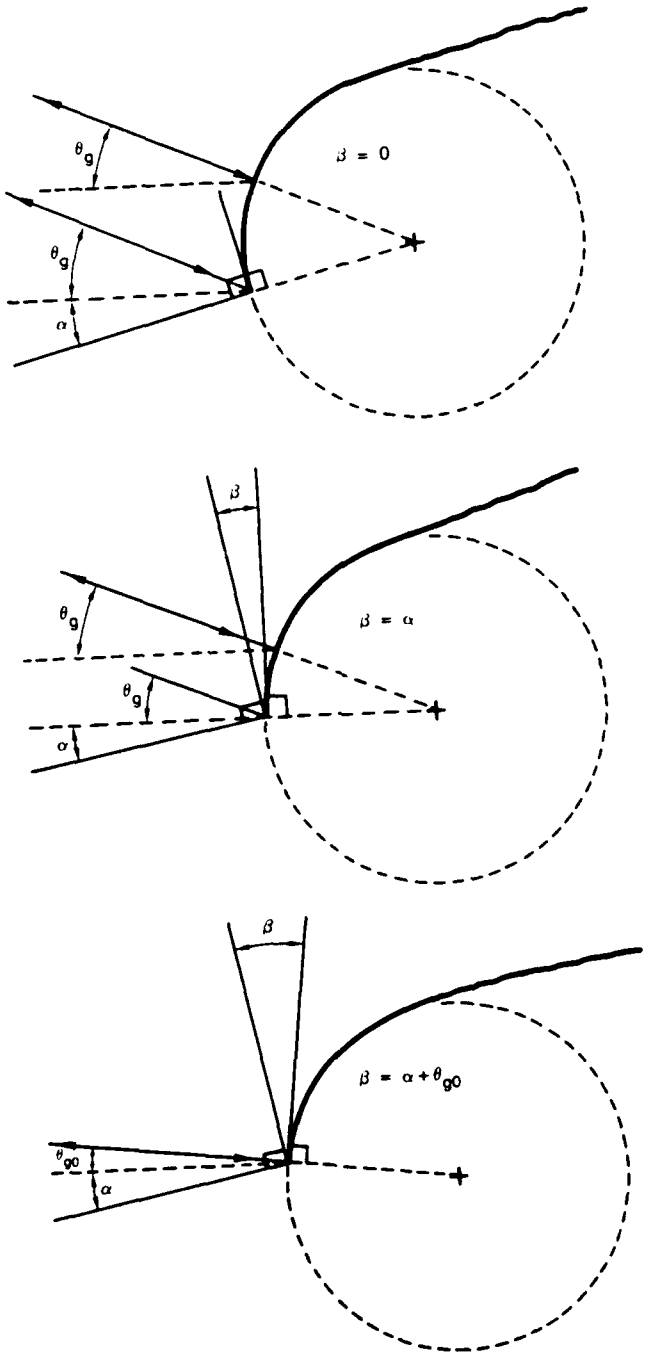

FIGURE 18. Cylindrical plume models suggested by Wetzel, 1986 (a) and modified versions suggested by Trizna, 1988 (b and c) to explain the grazing angle dependence of sea spikes for Atlantic data.

SUMMARY

Atlantic-Pacific Comparisons

The Pacific experiment results are significantly different than those of the north Atlantic experiment for the grazing angle region above 2 degrees, but are remarkably similar for lower grazing angles. This high angle difference occurs for all measures of sea spike radar cross section, Weibull B-parameters for both sea spikes and distributed scatter, and exponents of wind speed dependence for all parameters but the B-parameter. The distributed scatter results, on the other hand, demonstrated a grazing angle dependence for ranges not affected by STC that differed very little, except for being roughly 2.5 dB higher for the X-band Pacific data, and 3 dB lower for the S-band data.

In a general sense, one might consider the Pacific results as a lower limit case, appropriate to conditions of random seas. Similarly, the North Atlantic results can be considered as a current upper limit for well developed seas, with winds having blown for a significant time from the same direction over a long fetch. Higher air-sea temperature differences observed in much of the Atlantic data may be responsible for the higher sea spikes as well, although there did not appear to be a spread in data due to this variable in the Atlantic data. For cases of stronger winds over a longer fetch than encountered in the Atlantic data, one can expect a rise in the sea spike RCS beyond the current limit of the Atlantic results, although the scale sizes and lifetimes of weather systems might not present waves more fully developed than these very often. Hurricanes may produce higher winds, but the time over which they blow from the same direction may not be as long as encountered in the Atlantic data, except under conditions of stall in the weather system over a fixed area. Further understanding of the nature of the sea spike characteristics must now go beyond synoptic wind collection only. It requires a characterization of the directional wave spectrum and time series for an understanding of the time lag effect, as well as a better understanding of breaking waves in the open ocean and a determination of the deterministic scattering features responsible for the sea spike radar return discussed in the section on scattering model comparisons.

STC Corrections as a Possible Source of Error

Considering possible errors encountered, an increase in sea spike character at 2-deg cannot be due to improper STC corrections for the Atlantic data, as these corrections were applied only for the last two depression angles in that case. Similarly, STC corrections applied to the Pacific X-band median data results in the Pacific sea spike data for points 4 through 10 in Figs. 7 and 8 being re-registered to a similar level as for below 2-deg, resulting in a very consistent pair of plots, particularly considering the wide range of corrections applied to the X-band data here. The fact that these corrected results then have similar grazing angle dependencies as for the Atlantic data appear to confirm the strategy of deriving the STC corrections.

Errors in Wind Speed Measurement

Blanc (1986) has shown that errors in wind speed made using anemometers aboard ship are possible, due to flow distortion caused by the ship superstructure. Similar results have been documented aboard the Argus Island research tower by Thornwaite, et al, (1965). Such errors cause an overestimation of the open ocean wind speed, and are greatest for ship mounted anemometers on forward masts when the wind are from quadrants to the rear of the ship. As we have no knowledge of the ship's course relative to the wind for these data, such errors cannot be estimated. Assuming a uniform distribution of wind directions relative to the heading, the result would be a broadening of the wind measure to the higher side of the true value, resulting in a higher mean wind derived from the least-squares data fit. Future experiments are planned in which the relative wind direction will be known.

Analyses of scatterometer data have tended to compare with the wind friction velocity rather than wind speed. The friction velocity is a measure of the wind energy lost to generation of ocean waves, and is thought to be a more realistic parameter for surface roughness comparison. In the Atlantic analysis, some comparisons were made with friction velocity derived using the bulk method estimate, with several models for the drag coefficient used in least squares fitting. However, this method uses wind speed as an input and any errors in this variable translate to friction velocity. Future experiments are planned in which the dissipation method of friction velocity will be used, which uses a measure of the fluctuation spectrum of the wind, and is less affected by flow distortion than the wind speed magnitude is, used in the bulk method of friction velocity estimation.

The Weibull Distribution as an NRCS Model

The Weibull distribution of NRCS has never been derived from first principles, but was chosen as a result of previous work in which it provided a best fit to data when compared with other distributions. In the theoretical development of statistical radar scattering models, it is generally assumed that the sea surface distributions of wave slopes have Rayleigh distributions. (See, for example, section 3 of Fung and Lee's model development for the scatterometer NRCS.) This follows from the oceanographic observation that wave heights closely fit the Rayleigh distribution (Longuet-Higgins, 1975), and because the wave slope is just the derivative of the wave height, it should also be Rayleigh distributed. However, work by Forristall (1985) and more recently, Krogstad (1985), on the distribution of extreme waves for application to offshore structures, have shown that the Weibull distribution best describes the high-amplitude tails of extreme waves (very largest wave heights of the distribution), and quote values of the Weibull-B between 2.13 and 2.50. This is to be compared with our maximum and minimum values of 1.8 and 3.2 for distributed scatter over all grazing angles, and 0.8 and 2.3 for breaking waves, although such a comparison is not warranted without a detailed analysis of how the distribution of wave height samples translates to RCS samples. Suffice it to say that there is evidence for the Weibull distribution in oceanographic data that must be considered in development of sea surface radar cross section sample statistics.

Time Lags in Wave Direction

There is also evidence for time lags in the observation of the propagation direction of wave energy relative to changing wind direction. Recently Holthuijsen and Smith (1988) have studied empirically such lags, reporting values of the order of three hours for wave energy relative to the wind. They contrast this with the predictions of earlier work by Hasselmann, et al, (1980) for larger time lags associated with the peak frequency of the spectrum the order of 12 hours. As breaking waves might be expected to be associated with the longest waves, i.e., the peak frequency of the spectrum, Hasselmann's results are in line with our observations.

Sea-Spike Percentage Wind Speed Dependence

Finally, we comment on the lack of an analysis of wind speed dependence of sea spikes for the Pacific data. Such an analysis was done for the Atlantic data and showed a wind speed dependence similar to that observed in whitecap coverage studies. The plot of sea spike percentage for the Pacific data did not show a regular variation with wind speed as it did for the Atlantic data, even with the introduction of time lags, and thus was not pursued. It might be expected that similarity in the wind speed dependencies of sea spike percentage and white cap coverage percentages might only hold for relatively uniform seas as was observed in the Atlantic. For multi-modal seas (wave energy contributions from more than one direction) which must have persisted in the Pacific as evidenced by the time lag effects, such wind speed dependencies may be more complex. Jin Wu (private communication) suggests that open ocean wave breaking is dominated by winds tearing the tops off of waves. Thus, white cap coverage is expected to be associated with the current wind direction. However, the time lag used to register the radar data with wind speed forces attention to the long wave field, which is not in the same direction as the wind for much of our data. The variation of the intercept of the linear fit to the two regions of Fig. 3 is far more sensitive along the percentage axis than along the NRCS axis. The latter was used in determining the effective mean sea spike cross section, which did show a reasonable scatter when plotted versus wind speed. However, this stronger sensitivity in the percentage of sea spikes to wind speed causes too broad a scatter to make such comparisons with wind speed meaningful for these data.

REFERENCES

Blanc, T., Superstructure flow distortion correction for wind speed and directions - measurements made from Tarawa Class (LHA1-LHA5) ships, NRL Report 9005, Oct. 1986.

de Loor, G.P., and P. Hoogeboom, Radar backscatter measurements from platform Noordwijk in the North Sea, IEEE J. Ocean Engin., Vol. OE-7, pp. 15-20, 1982.

Feindt, F., J. Shroter and W. Alpers, Measurement of the ocean wave-radar modulation transfer function at 35 GHz from a sea-based platform in the North Sea, J. Geophys. Res. 91, 9701-9708, 1986.

Forristall, G.Z., On the statistics of wave heights in a storm,JGR, Vol. 83, pp. 2353-2358, 1978.

Fung, A.K., and K.K. Lee, A semi-empirical sea spectrum model for scattering coefficient estimation, IEEE J. Ocean Eng., Vol. OE-7, pp. 166-176, 1982.

Hasselmann, D.E., M. Dunkel, J.A. Ewing, Directional wave spectra observed during JONSWAP, J. Phys. Ocean., Vol. 10, pp. 1264- 1280, 1980.

Holthuijsen, L.H., and D.R. Smith, An evaluation of model estimates of ocean wave directions, Ocean Eng., Vol. 15,pp. 127-137, 1988.

Krogstad, H.E., Height and period distributions of extreme waves, Applied Ocean Res., Vol. 7, pp. 158-165, 1985.

Longuet-Higgins, On the joint distribution of periods and amplitudes of sea waves, JGR, Vol. 80, p. 2688, 1975.

Neumann, G., On ocean wave spectra and a new method of forecasting wind generated sea, Beach Erosion Board,
U.S. Army Corps of Engineers, Tech Memo #43, 1953.

Okuda, K., S. Kawai and Y. Toba, Measurement of skin friction distribution along the surface of wind waves, J. Oceanogr. Soc. Japan 33, 190-198, 1977.

Sun, S.-C. and Jin Wu, On airflow boundary layer above the profile of long waves, J. Phys. Oceanogr. 14, 1811-1815, 1984.

Thornwaite, C.W., W.J. Superior, and R.T. Field, Disturbances of airflow around Argus Island near Bermuda, JGR, Vol. 70, pp. 6047-6052, 1965.

Trizna, D. B., Measurement and interpretation of North Atlantic Ocean marine radar sea scatter, NRL Report 9099, April, 1988.

Trizna, D.B. and Jin Wu, The modulation transfer function for radar sea scatter - a two-source model, (Submitted to JGR).

Wetzel, L., On microwave scattering by breaking waves, in Wave Dynamics and Radio Probing of the Ocean Surface, O. M. Phillips and K. Hasselmann, eds., Plenum Press, New York, 273-284, 1986.

Wu, Jin, Oceanic whitecaps and sea state, JPO, 9, pp.1064-1068, 1979.